

2 **Finite element analyses of human vertebral bodies embedded in**
3 **polymethylmethacrylate or loaded via the hyperelastic intervertebral disc**
4 **models provide equivalent predictions of experimental strength**

5 Yongtao Lu^{a,*1}, Ghislain Maquer^{b,1}, Oleg Museyko^c, Klaus Püschel^d, Klaus
6 Engelke^c, Philippe Zysset^b, Michael Morlock^a, Gerd Huber^a

7 ^aInstitute of Biomechanics, TUHH Hamburg University of Technology, Hamburg,
8 Germany

9 ^bInstitute of Surgical Technology & Biomechanics, University of Bern, Bern,
10 Switzerland

11 ^cInstitute of Medical Physics, University of Erlangen-Nuremberg, Erlangen,
12 Germany

13 ^dDepartment of Legal Medicine, University Medical Center Hamburg-Eppendorf,
14 Hamburg, Germany.

15 ¹ The first two authors contributed equally to this work
16

17 **Address of corresponding author:**

18 Yongtao Lu Ph.D
19 Institute of Biomechanics
20 TUHH Hamburg University of Technology
21 Denickestraße 15
22 21073 Hamburg, Germany
23 Phone: +49 (0) 40 42878 3184
24 Fax: +49 (0) 40 42878 2996
25 Email:yongtao.lu@tuhh.de

26 **Abstract:** 249

27 **Word count for the main text (Introduction to discussion):** 2051

28 **Number of tables:** 2

29 **Number of figures:** 4

1 **Abstract**

2 Quantitative computer tomography (QCT)-based finite element (FE) models of
3 vertebral body provide better prediction of vertebral strength than dual energy X-
4 ray absorptiometry. However, most models were validated against compression of
5 vertebral bodies with endplates embedded in polymethylmethacrylate (PMMA).
6 Yet, loading being as important as bone density, the absence of intervertebral disc
7 (IVD) affects the strength. Accordingly, the aim was to assess the strength
8 predictions of the classic FE models (vertebral body embedded) against the *in vitro*
9 and *in silico* strengths of vertebral bodies loaded via IVDs. High resolution
10 peripheral QCT (HR-pQCT) were performed on 13 segments (T11/T12/L1). T11
11 and L1 were augmented with PMMA and the samples were tested under a 4° wedge
12 compression until failure of T12. Specimen-specific model was generated for each
13 T12 from the HR-pQCT data. Two FE sets were created: FE-PMMA refers to the
14 classical vertebral body embedded model under axial compression; FE-IVD to their
15 loading via hyperelastic IVD model under the wedge compression as conducted
16 experimentally. Results showed that FE-PMMA models overestimated the
17 experimental strength and their strength prediction was satisfactory considering the
18 different experimental set-up. On the other hand, the FE-IVD models did not prove
19 significantly better (Exp/FE-PMMA: $R^2 = 0.68$; Exp/FE-IVD: $R^2 = 0.71$, $p = 0.84$).
20 In conclusion, FE-PMMA correlates well with *in vitro* strength of human vertebral
21 bodies loaded via real IVDs and FE-IVD with hyperelastic IVDs do not
22 significantly improve this correlation. Therefore, it seems not worth adding the
23 IVDs to clinical models until fully validated patient-specific IVD models become
24 available.

25 **Keywords:** Human vertebra, finite element prediction, mechanical testing, failure
26 strength, intervertebral disc

1 **1. Introduction**

2 Vertebral failure constitutes a serious health problem because of its association
3 with back pain, disability and the impairment of life quality (Lips et al., 1999). The
4 risk of vertebral failure is currently commonly determined by a wide range of bone
5 mineral density (BMD) measurements, e.g. the areal BMD (aBMD) and the
6 volumetric BMD (vBMD). However, studies showed only 50% to 70% of the
7 variability in vertebral strength can be predicted by BMD measurements (Ammann
8 and Rizzoli, 2003; Lochmüller et al., 2002). In order to improve the vertebral
9 failure prediction, attention has been paid to other techniques, e.g. the finite
10 element (FE) method, which can represent the bone microstructure not captured by
11 the BMD measurements (Faulkner et al., 1991). Consequently, the FE modelling
12 approach has recently gained increasing interest in predicting vertebral strength
13 (Chevalier et al., 2010; Dall’Ara et al., 2012; Imai et al., 2008) and has shown better
14 failure prediction than aBMD (Wang et al., 2012) and vBMD (Crawford et al.,
15 2003) alone.

16 The vertebral strength was only assessed using vertebral bodies, whose
17 endplates were either removed or embedded in polymethylmethacrylate (PMMA)
18 to avoid uncertainties regarding the degree of degeneration of the elderly
19 intervertebral disc (IVD) (Buckley et al., 2007; Crawford et al., 2003; Dall’Ara et
20 al., 2012). These boundary conditions, although equivalent (Maquer et al. 2012a),

1 are not appropriate for the study of failures in vertebral endplate, which is a major
2 failure pattern in the elderly (Rao and Singrakhia, 2003). On the other hand, the
3 failure mechanisms in the vertebra are altered in the absence of IVD (Hussein et al.,
4 2013), which plays an important role in transferring and distributing the
5 compressive load (Adams et al., 2006). Moreover, the IVD stiffness affects the
6 overall ductility of the vertebral bodies (Nekkanty et al., 2010) and the vertebral
7 failure site (Pollintine et al., 2004). Finally, numerical simulations showed that FE
8 models of embedded vertebral body provided different strength and failure patterns
9 compared to models bonded to healthy IVDs (Maquer et al., 2012b). Accordingly,
10 the aim of this study was to investigate whether the classic vertebral body
11 embedded axial compression FE models (referred as FE-PMMA models) are still
12 valid for the prediction of *in vitro* strength of human vertebral body loaded via
13 IVDs under a wedge compression and if the predictions can be improved using FE
14 spinal models with hyperelastic IVDs and *in vitro* consistent loading (FE-IVD
15 models).

16

17 **2. Materials and methods**

18 *2.1. In vitro* mechanical testing

19 In this study, 13 T11/T12/L1 spinal segments, without failure, nor osteophytes,
20 were received. The donors were postmenopausal females with a mean age of $79.9 \pm$

1 7.9 years [range: 67-90]. DXA bone densitometry (Lunar Prodigy, Lunar
2 Corporation, Madison, WI, USA) was performed for the lumbar spine and both
3 proximal femurs and subsequently all donors were diagnosed with osteoporosis
4 according to the World Health Organization definition with a lumbar or femoral T-
5 score of -2.5 or less. The segments were scanned while frozen using a HR-pQCT
6 scanner (XtremeCT, Scanco Medical AG, Brüttisellen, Switzerland) with an image
7 voxel size of $82 \mu\text{m}^3$.

8 Following the standard procedures (Skrzypiec et al., 2013), the specimens were
9 stored and prepared for mechanical testing. The spinal facet joints were removed
10 for the loading to be only transferred via the IVDs. Failures in T11 and L1 were
11 avoided by replacing the cancellous bone with PMMA (Technovit 4004, Heraeus
12 Kulzer, Wehrheim, Germany). The specimens were embedded in metal cups, such
13 that the mid-transverse planes of T12 were horizontal and in neutral posture (no
14 bending).

15 The embedded specimens were mounted in a computer-controlled servo-
16 hydraulic materials testing machine (MTS Bionix 858.2, Eden Prairie, MN, US).
17 Axial force was applied for 15 min as a preconditioning to account for the post-
18 mortem swelling (Hongo et al., 2008). The applied force was subject-specific and
19 calculated based on the donor's body weight (300 N for a 70 kg person in standing
20 position) (Nachemson, 1966). After preconditioning, a 4° anterior-posterior wedge

1 was applied to T11 to induce a wedge fracture loading condition for T12 (Adams et
2 al. 2006) (Figure 1). An x-y-table was installed between the wedge and the actuator
3 to allow free translations in the transverse plane and so to prevent coupled shear
4 loading during assembly.

5 A quasi static compression loading of 0.1 mm/s was then applied (Brinckmann
6 et al., 1989) and the x-y-table was locked to prevent extensive spinal anterior-
7 posterior movements, eventually leading to rupture between the posterior regions of
8 the IVD and the vertebral body. The test was performed until a dramatic drop of
9 force (>15% of the peak force) was observed on the load-displacement curve. The
10 maximal force measured was defined as the vertebral failure load (F^{exp}).

11 2.2. Finite element model

12 Subject-specific FE models of T12 vertebral bodies were created based on the HR-
13 pQCT data. T11 and L1 were not modelled as their deformations were negligible
14 due to PMMA augmentations. T12 models were created using an in-house software
15 (MedTool, Institute of Lightweight Design and Structural Biomechanics, Vienna
16 University of Technology, Vienna, Austria) (Pahr and Zysset, 2008). Quadratic
17 wedge (C3D15) and tetrahedral elements (C3D10) were defined for the cortex and
18 the trabecular bone, respectively, as described in Maquer et al. (2012b). The
19 anisotropic elastic-plastic-damage model from Schwiedrzik and Zysset (2013) was

1 chosen to simulate the mechanical behaviour of each bone elements based on the
2 local bone content and trabecular morphology.

3 The solid volume for each IVD was extruded from the superior and inferior
4 endplate surfaces of its adjacent vertebrae (HyperMesh, Version 11.0, Altair
5 Engineering Inc., Troy, MI, USA). The endplate surfaces were extracted from the
6 meshes of T12 or reconstructed from the automatic segmentation of T11 and L1
7 (MIAF-Spine, Institute of Medical Physics, University of Erlangen, Germany)
8 (Mastmeyer et al., 2006). The IVD volume was discretized with C3D10 and then
9 the elements were organised into annulus fibrosus (AF) and nucleus pulposus (NP)
10 according to the transverse sectional view (Figure 2).

11 Two IVD materials were used to generate either the classical FE-PMMA
12 models or the FE-IVD models (Figure 3). Hence, linear elastic modulus of 2300
13 MPa and Poisson's ratio of 0.3 [Heraeus Kulzer GmbH, Wehrheim, Germany]
14 were applied to both NP and AF elements for FE-PMMA. For FE-IVD, Mooney-
15 Rivlin model was defined for NP and fibre-reinforced hyperelastic model
16 (Moramarco et al., 2010) was chosen for AF. The material parameters are C_{10} , C_{01} ,
17 C_{20} , K_1 , K_2 and D , where, C_{10} , C_{01} and C_{20} are related to the ground substance; K_1
18 and K_2 are parameters characterizing the behaviour of the collagen fibres; D is the
19 incompressibility modulus. Two families of fibres with the angulations of $\pm 30^\circ$

1 (relative to the transverse plane) (Cassidy et al., 1989) were defined in AF and both
2 families were acting only in tension.

3 Three different grades of IVD degeneration (healthy, moderately and severely)
4 were identified from the IVD transverse sectional view (Thompson et al., 1990)
5 and simulated in FE-IVD models. It was assumed that IVD degeneration had no
6 effect on AF material properties (Schmidt et al., 2007), which were taken from
7 literature (Moramarco et al., 2010) (Table 1). The material properties for healthy
8 NP were also taken from literature (Schmidt et al., 2007) (Table 1). The
9 dehydration of NP was simulated by changing the incompressibility modulus,
10 whose value was 0.0005 MPa^{-1} for healthy IVD and corresponded to that of AF for
11 severely degenerated IVD (Rohlmann et al., 2006). The incompressibility modulus
12 for moderately degenerated IVD was linearly interpolated (Rohlmann et al., 2006).
13 The stiffening of NP was simulated by modifying the values of C_{10} and C_{01}
14 (Schmidt et al., 2007).

15 The bone and AF constitutive laws were implemented into Abaqus (Version
16 6.12, Dassault Systemes SIMULIA Ltd, Providence, RI, USA) via user defined
17 material subroutine. To simulate the axial compression on FE-PMMA models, the
18 bottom nodes from the inferior PMMA block were fully constrained while an axial
19 displacement of 4.0 mm was prescribed to the nodes of the superior PMMA layer.
20 To mimic the experimental loading applied to FE-IVD models, the bottom nodes

1 from the inferior IVD were fully constrained. A 2-stage loading was conducted on
2 the cranial nodes of the superior IVD: a first step consisting in a 4° forward
3 bending was followed by an axial displacement of 4.0 mm to ensure failure of T12.
4 Non-linear analyses were performed and the FE failure loads (F_{PMMA}^{FE} and F_{IVD}^{FE})
5 were computed as the maximal force.

6 2.3. Statistical analysis

7 A paired two-tailed t-test was used to compare the vertebral failure loads with the
8 FE predictions. Regression equations, the coefficients of determination (R^2) and
9 root mean squared errors (RMS) were computed for the linear correlations of the
10 vertebral failure load with FE predictions (Crawford et al., 2003). Analyses were
11 performed using PASW statistics 18.0 (SPSS Inc., Chicago, IL, USA) and the
12 probability of type I error was set to $\alpha = 0.05$, i.e. $p < 0.05$ was considered
13 statistically significant.

14

15 3. Results

16 Compared to the experimental failure loads, FE predicted loads were 12% lower in
17 FE-IVD group (mean \pm SD, 2.09 ± 0.48 kN vs. 1.84 ± 0.47 kN, $p = 0.005$) and 18%
18 higher in FE-PMMA group (2.09 ± 0.48 kN vs. 2.46 ± 0.62 kN, $p = 0.002$) (Table
19 2). Both predicted failure loads were significantly correlated (FE-IVD/FE-PMMA:
20 $R^2 = 0.94$) and showed similar correlation with the experimental vertebral strength

1 (Exp/FE-PMMA: $R^2 = 0.68$; Exp/FE-IVD: $R^2 = 0.71$) (Figure 4). No significant
2 difference was detected between the absolute value of the residuals from the FE-
3 IVD and FE-PMMA regression models ($p = 0.84$).

4

5 **4. Discussion**

6 The study confirmed that the PMMA embedding is providing a higher vertebral
7 strength, which is probably because a larger portion of the load is carried by the
8 cortex (Homminga et al. 2001, Maquer et al. 2012b). Yet, despite different loading
9 conditions, the FE-PMMA models provided a satisfactory prediction of the failure
10 loads of vertebral bodies under a 4° wedge compression via IVDs and showed the
11 same predictive power as the FE-IVD models ($R^2 = 0.68$ vs. 0.71). FE-PMMA
12 models are more reproducible by avoiding approximation regarding the degree of
13 elderly IVD's degeneration (Dall'ara et al. 2012), computationally more efficient
14 and ease of clinical implementation. This essentially indicates that FE-PMMA
15 models are satisfactory (Buckley et al., 2006), although rigid boundary conditions
16 are prescribed to the endplates and axial compression conducted. This agreed with
17 Yang et al.'s (2012) study where it was found that a 5° forward flexion does not
18 significantly affect the spatial distribution of stress within the vertebral body.

19 The hyperelastic IVD model, although reasonable for simulation of the
20 kinematic of the spine (Moramarco et al. 2010), and the instantaneous response of
21 IVD (Jones, et al., 2008), is hardly applicable to simulate the *in vitro* load transfer

1 to the endplates. Indeed, the accuracy of the vertebral strength predictions is highly
2 dependent on the degree of simplification of those IVD models (Jones, et al.,
3 2008). While the latest image-based bone models (Pahr, et al., 2012; Hosseini, et al.,
4 2012) move towards patient-specific modelling (Gefen, 2012), such step is still to
5 be taken regarding the IVD modelling. In this study, IVD shape was deduced from
6 the endplates of the neighbouring vertebral bodies (Moramarco, et al., 2010;
7 Homminga, et al., 2012). MRI is able to accurately capture the IVD morphology,
8 but the IVD geometry in most FE models are idealised and rarely based on MRI
9 data (Moramarco, et al., 2010; Schmidt, et al., 2007). The distinction NP/AF is
10 hardly possible with degenerated IVDs (Ellingson et al. 2012). Moreover, discrete
11 degrees of degeneration were simulated as commonly done in most degeneration
12 schemes (Thompson et al. 1990, Pfirmann et al. 2001). Considering the range of
13 alterations observed in moderately to highly degenerative IVDs and that the elderly
14 IVDs in this study were likely having different degenerative levels, a discretization
15 constitutes a considerable simplification. Quantitative MRI data correlates with the
16 IVD's mechanical properties (Périé et al. 2006, Campana et al. 2011, Maquer et al.
17 2014) but such information have not been applied to an IVD model.

18 Hence, despite the small sample size, this study showed that the vertebral
19 strength computed by FE-PMMA models correlated well with the *in vitro* strength
20 of human vertebral bodies loaded via real IVDs. The FE-IVD models did not

1 significantly improve this correlation, probably due to a lack of patient-specific
2 disc models. In conclusion, for clinical assessment of strength, it is probably not
3 worth the trouble of adding the discs to vertebral body models until fully validated
4 patient-specific IVD models become available.

5

6 **Ethical approval**

7 Ethical approval has been obtained from the Ethics Committee of the Hamburg
8 Chamber of Physicians (PV3486).

9

10 **Acknowledgement**

11 This work was supported by the German Federal Ministry of Education and
12 Research (BMBF) under Grant 01EC1005 and by the Swiss National Science
13 Foundation (SNF), grant n°483 325230_147153. The authors would like to
14 acknowledge Kay Sellenschloh and Matthias Vollmer for their help in the
15 mechanical testing, Imke Fiedler for assisting in the FE sample studies, Dr. med
16 Matthias Krause for performing the HR-pQCT scans, Prof. Michael Amling for the
17 support with the ethics approval and Dr. Birgit Wulff for counselling the next of
18 kin.

19

20 **References:**

1 Adams, M.A., Pollintine, P., Tobias, J.H., Wakley, G.K., Dolan, P., 2006.
2 Intervertebral disc degeneration can predispose to anterior vertebral failures in
3 the thoracolumbar spine. *Journal of Bone and Mineral Research* 21 (9), 1409–
4 1416.

5 Ammann, P., Rizzoli, R., 2003. Bone strength and its determinants. *Osteoporosis*
6 *International* 14 (S3), S13–18.

7 Brinckmann, P., Biggemann, M., Hilweg, D., 1989. Prediction of the compressive
8 strength of human lumbar vertebrae. *Clinical Biomechanics* 4 (S2), 1–27.

9 Buckley, J.M., Leang, D.C., Keaveny, T.M., 2006. Sensitivity of vertebral
10 compressive strength to endplate loading distribution. *Journal of*
11 *Biomechanical Engineering* 128(5), 641– 646.

12 Buckley, J.M., Loo, K., Motherway, J., 2007. Comparison of quantitative computed
13 tomography-based measures in predicting vertebral compressive strength.
14 *Bone* 40 (3), 767–774.

15 Campana, S., Charpail, E., De Guise, J. A., Rillardon, L., Skalli, W., Mitton, D.,
16 2011. Relationships between viscoelastic properties of lumbar intervertebral
17 disc and degeneration grade assessed by MRI. *Journal of the Mechanical*
18 *Behavior of Biomedical Materials* 4(4), 593-599.

19 Cassidy, J.J., Hiltner, A., Baer, E., 1989. Hierarchical structure of the intervertebral
20 disc. *Connective Tissue Research* 23(1), 75-88.

21 Chevalier, Y., Quek, E., Borah, B., Gross, G., Stewart, J., Lang, T., et al., 2010.
22 Biomechanical effects of teriparatide in women with osteoporosis treated
23 previously with alendronate and risedronate: results from quantitative
24 computed tomography-based finite element analysis of the vertebral body.
25 *Bone* 46 (1), 41–48.

- 1 Crawford, R.P., Cann, C.E., Keaveny, T.M., 2003. Finite element models predict in
2 vitro vertebral body compressive strength better than quantitative computed
3 tomography. *Bone* 33 (4), 744–750.
- 4 Dall'Ara, E., Schmidt, R., Pahr, D., Varga, P., Chevalier, Y., Patsch, J., Kainberger,
5 F., Zysset, P., 2010. A nonlinear finite element model validation study based
6 on a novel experimental technique for inducing anterior wedge-shape fractures
7 in human vertebral bodies in vitro. *Journal of Biomechanics* 43(12), 2374-
8 2380.
- 9 Dall'Ara, E., Pahr, D., Varga, P., Kainberger, F., Zysset, P., 2012. QCT-based
10 finite element models predict human vertebral strength in vitro significantly
11 better than simulated DEXA. *Osteoporosis International* 23 (2), 563–572.
- 12 Ellingson, A.M., Mehta, H., Polly, D.W., Ellermann, J., Nuckley, D.J., 2013, Disc
13 degeneration assessed by quantitative T2* correlated with functional lumbar
14 mechanics, *Spine* 38(24), E1533-E1540.
- 15 Faulkner, K.G., Cann, C.E., Hasegawa, B.H., 1991. Effect of bone distribution on
16 vertebral strength: assessment with patient-specific nonlinear finite element
17 analysis. *Radiology* 179(3), 669-674.
- 18 Gefen, A., 2012. *Patient-specific Modeling in Tomorrow's Medicine* (Vol. 9).
19 Springer.
- 20 Homminga, J., Weinans, H., Gowin, W., Felsenberg, D., & Huiskes, R. 2001.
21 Osteoporosis changes the amount of vertebral trabecular bone at risk of
22 fracture but not the vertebral load distribution. *Spine*, 26(14), 1555-1560.
- 23 Homminga, J., Aquarius, R., Bultink, V. E., Jansen, C. T., Verdonschot, N., 2012.
24 Can vertebral density changes be explained by intervertebral disc degeneration?
25 *Medical Engineering and Physics* 34(4), 453-458.
- 26 Hongo, M., Gay, R.E., Hsu, J.T., Zhao, K.D., Ilharreborde, B., Berglund, L.J., et al.,
27 2008. Effect of multiple freeze-thaw cycles on intervertebral dynamic motion

1 characteristics in the porcine lumbar spine. *Journal of Biomechanics* 41 (4),
2 916–920.

3 Hosseini, H. S., Pahr, D. H., Zysset, P. K., 2012. Modeling and experimental
4 validation of trabecular bone damage, softening and densification under large
5 compressive strains. *Journal of the Mechanical Behavior of Biomedical*
6 *Materials* 15, 93-102.

7 Hussein, A.I., Mason, Z.D., Morgan, E.F., 2013. Presence of intervertebral discs
8 alters observed stiffness and failure mechanisms in the vertebra. *Journal of*
9 *Biomechanics* 46, 1683-1688.

10 Imai, K., Ohnishi, I., Yamamoto, S., Nakamura, K., 2008. In vivo assessment of
11 lumbar vertebral strength in elderly women using computed tomography-
12 based nonlinear finite element model. *Spine* 33 (1), 27–32.

13 Jones, A. C., Wilcox, R. K., 2008. Finite element analysis of the spine: towards a
14 framework of verification, validation and sensitivity analysis. *Medical*
15 *Engineering and Physics* 30(10), 1287-1304.

16 Lips, P., Cooper, C., Agnusdei, D., Caulin, F., Egger, P., Johnell, O., et al., 1999.
17 Quality of life in patients with vertebral failures: Validation of the quality of
18 life questionnaire of the European Foundation for Osteoporosis (QUALEFFO).
19 Working Party for Quality of Life of the European Foundation for
20 Osteoporosis. *Osteoporosis International* 10 (2), 150–160.

21 Lochmüller, E.M., Bürklein, D., Kuhn, V., Glaser, C., Müller, R., Glüer, C.C., et al.,
22 2002. Mechanical strength of the thoracolumbar spine in the elderly:
23 prediction from in situ dual-energy X-ray absorptiometry, quantitative
24 computed tomography (QCT), upper and lower limb peripheral QCT, and
25 quantitative ultrasound. *Bone* 31 (1), 77–84.

26 Maquer, G., Dall'Ara, E., Zysset, P. K., 2012a. Removal of the cortical endplates
27 has little effect on ultimate load and damage distribution in QCT-based voxel

1 models of human lumbar vertebrae under axial compression. *Journal of*
2 *Biomechanics* 45(9), 1733-1738.

3 Maquer, G., Schwiedrzik, J., Zysset, P.K., 2012b. Embedding of human vertebral
4 bodies leads to higher ultimate load and altered damage localisation under
5 axial compression. *Comput Methods Biomech Biomed Engin.*
6 <http://dx.doi.org/10.1080/10255842.2012.744400>. (Epub ahead of print).

7 Maquer, G., Brandejsky, V., Benneker, L. M., Watanabe, A., Vermathen, P., Zysset,
8 P. K., 2014. Human intervertebral disc stiffness correlates better with the Otsu
9 threshold computed from axial T2 map of its posterior annulus fibrosus than
10 with clinical classifications. *Medical Engineering and Physics* 36(2), 219-225.

11 Mastmeyer, A., Engelke, K., Fuchs, C., Kalender, W.A., 2006. A hierarchical 3D
12 segmentation method and the definition of vertebral body coordinate systems
13 for QCT of the lumbar spine. *Medical Image Analysis* 10, 560-577.

14 Moramarco, V., Perez del Palomar, A., Pappalettere, C., Doblare, M., 2010. An
15 accurate validation of a computational model of a human lumbosacral segment.
16 *Journal of Biomechanics* 43 (2), 334-342.

17 Nachemson, A., 1966. The load on lumbar disks in different positions of the body.
18 *Clinical Orthopaedics and Related Research* 45, 107-122.

19 Nekkanty, S., Yerramshetty, J., Kim, D., Zael, R., Johnson, E., Cody, D.D., et al.,
20 2010. Stiffness of the endplate boundary layer and endplate surface
21 topography are associated with brittleness of human whole vertebral bodies.
22 *Bone* 47 (4), 783–789.

23 Pahr, D.H., Zysset, P.K., 2008. From high-resolution CT data to finite element
24 models: development of an integrated modular framework. *Computer*
25 *Methods in Biomechanics and Biomedical Engineering* 12 (1), 45–57.

26 Pahr, D. H., Dall'Ara, E., Varga, P., Zysset, P. K., 2012. HR-pQCT-based
27 homogenised finite element models provide quantitative predictions of

1 experimental vertebral body stiffness and strength with the same accuracy as
2 μ FE models. *Computer Methods in Biomechanics and Biomedical*
3 *Engineering*, 15(7), 711-720.

4 Perie, D., Iatridis, J. C., Demers, C. N., Goswami, T., Beaudoin, G., Mwale, F.,
5 Antoniou, J., 2006. Assessment of compressive modulus, hydraulic
6 permeability and matrix content of trypsin-treated nucleus pulposus using
7 quantitative MRI. *Journal of Biomechanics* 39(8), 1392-1400.

8 Pfirrmann, C. W., Metzdorf, A., Zanetti, M., Hodler, J., Boos, N., 2001. Magnetic
9 resonance classification of lumbar intervertebral disc degeneration. *Spine*
10 26(17), 1873-1878.

11 Pollintine, P., Dolan, P., Tobias, J.H., Adams, M.A., 2004. Intervertebral disc
12 degeneration can lead to ‘stress-shielding’ of the anterior vertebral body: a
13 cause of osteoporotic vertebral failure? *Spine* 29 (7), 774–782.

14 Rao, R.D., Singrakhia, M.D., 2003. Painful osteoporotic vertebral failure:
15 pathogenesis, evaluation, and roles of vertebroplasty and kyphoplasty in its
16 management. *The Journal of Bone and Joint Surgery American Volume*. 85
17 (10), 2010–2022.

18 Rohlmann, A., Zander, T., Schmidt, H., Wilke, H.J., Bergmann, G., 2006. Analysis
19 of the influence of disc degeneration on the mechanical behaviour of a lumbar
20 motion segment using the finite element methods. *Journal of Biomechanics* 39
21 (13), 2484 -2490.

22 Schmidt, H., Kettler, A., Rohlmann, A., Claes, L., Wilke, H.J., 2007. The risk of
23 disc prolapses with complex loading in different degrees of disc degeneration
24 – A finite element analysis. *Clinical Biomechanics* 22 (9), 988–998.

25 Schwiedrzik, J.J., Zysset, P.K., 2013. An anisotropic elastic viscoplastic damage
26 model for bone tissue. *Biomechanics and Modeling in Mechanobiology* 12 (2),
27 201–213.

1 Skrzypiec, D.M., Bishop, N.E., Klein, A., Pueschel, K., Morlock, M.M., Huber, G.,
2 2013. Estimation of shear load sharing in moderately degenerated human
3 lumbar spine. *Journal of Biomechanics* 46(4), 651-657.

4 Thompson, J.P., Pearce, R.H., Schechter, M.T., Adams, M.E., Tsang, I.K., Bishop,
5 P.B., 1990. Preliminary evaluation of a scheme for grading the gross
6 morphology of the human intervertebral disc. *Spine* 15 (5), 411–415.

7 Wang, X., Sanyal, A., Cawthon, P.M., Palermo, L., Jekir, M., Christensen, J., et al.,
8 2012. Prediction of new clinical vertebral failures in elderly men using finite
9 element analysis of CT scans. *Journal of Bone and Mineral Research* 27 (4),
10 808–816.

11 Yang, H., Nawathe, S., Fields, A.J., and Keaveny, T.M. 2012. Micromechanics of
12 the human vertebral body for forward flexion. *Journal of biomechanics*,
13 45(12), 2142-2148.

14
15

1 **Table 1.** Material properties for different grades of intervertebral disc

		healthy	moderately degenerated	severely degenerated	Reference
nucleus pulposus	C_{10} [MPa]	0.12	0.17	0.19	(Schmidt et al. 2007, Rolhmann et al. 2006)
	C_{01} [MPa]	0.03	0.041	0.045	
	D [MPa ⁻¹]	0.0005	0.158	0.3	
annulus fibrosus	C_{10} [MPa]	0.1			(Moramarco et al., 2010)
	C_{20} [MPa]	2.5			
	D [MPa ⁻¹]	0.3			
	K_1 [MPa]	1.8			
	K_2	11.0			

2

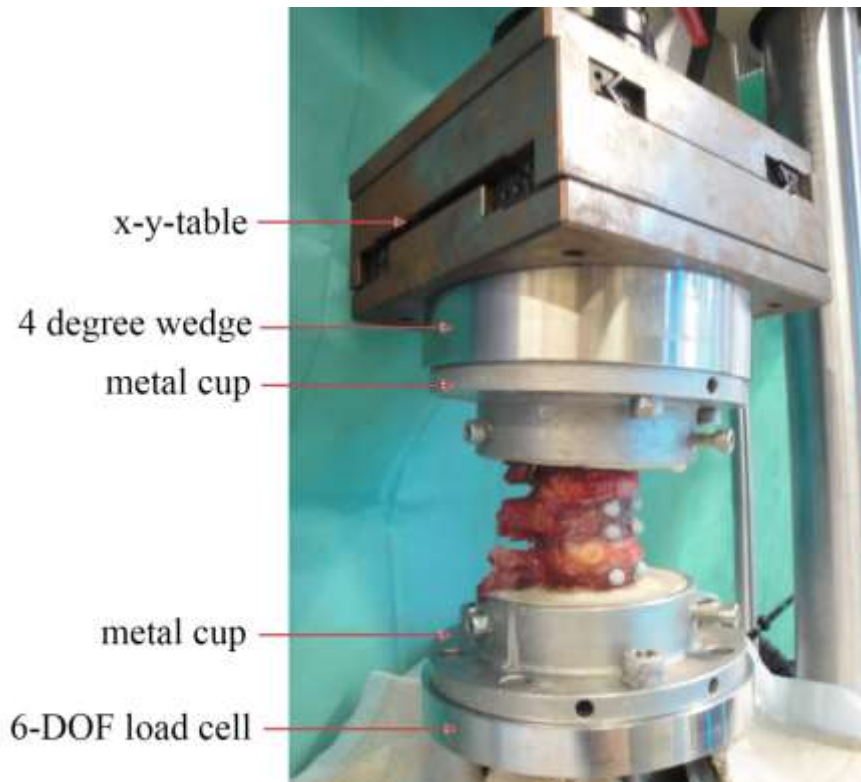
3

4 **Table 2.** Donor information and failure load data for the 13 T12 vertebral bodies

Parameter	Mean \pm SD	Range
Age [year]	79.9 \pm 7.8	65 – 90
Body weight [kg]	54.9 \pm 15.8	41 – 94.7
F_{IVD}^{FE} [kN]	1.84 \pm 0.47	1.03 – 2.50
F_{PMMA}^{FE} [kN]	2.46 \pm 0.62	1.39 – 3.40
F^{exp} [kN]	2.09 \pm 0.48	1.01 – 2.73

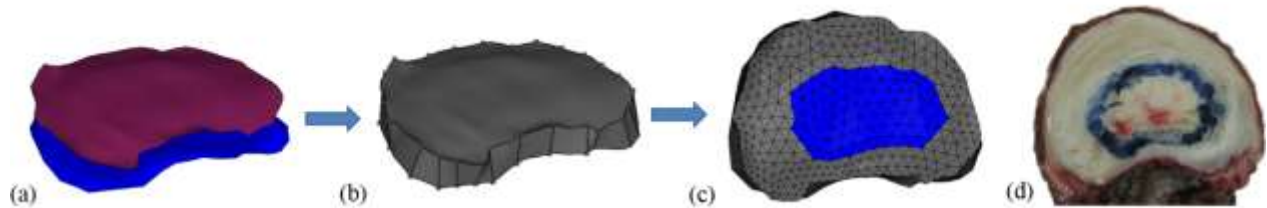
5

6



1

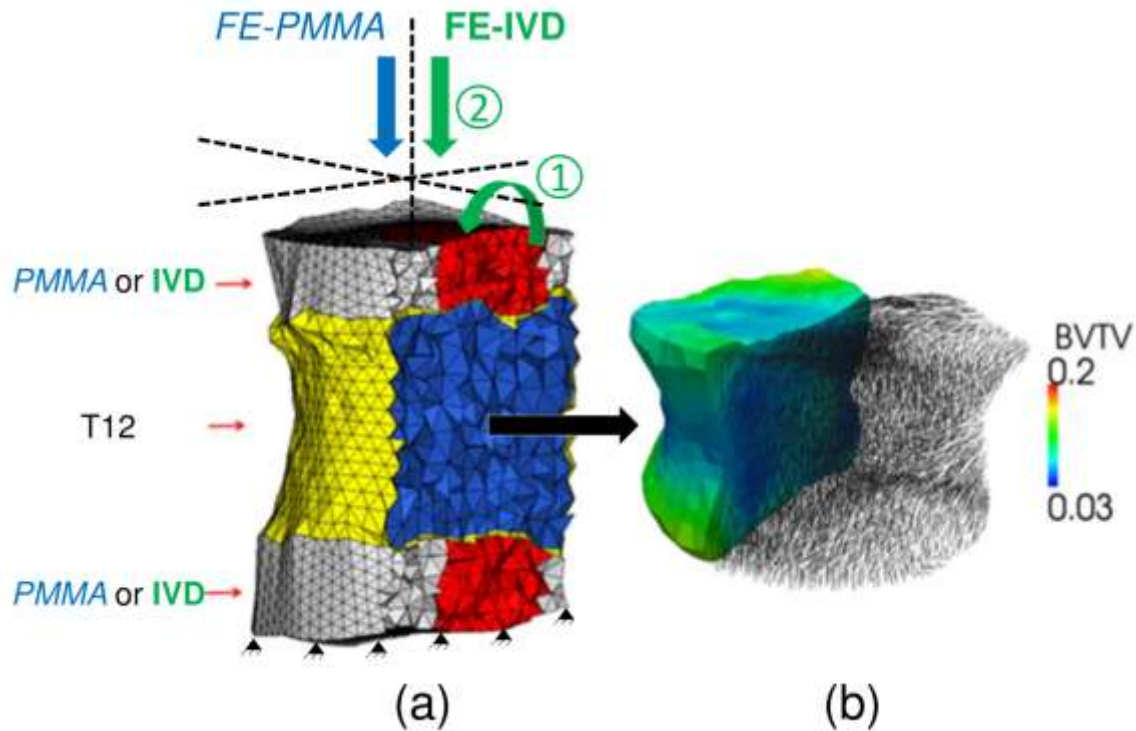
2 **Figure 1.** Mechanical testing setup for a representative 3-vertebra segment with
 3 disconnected facet joints.



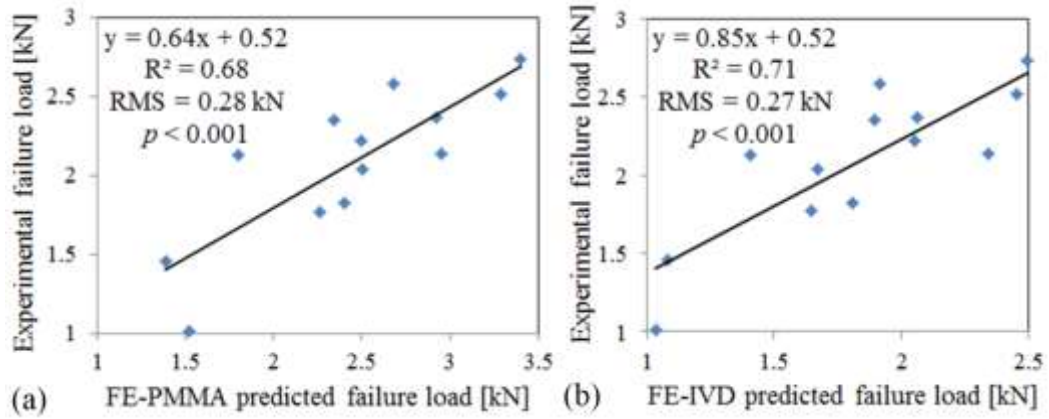
4

5 **Figure 2.** Generation of the finite element intervertebral disc (IVD) and
 6 comparison with the transverse sectional view of corresponding IVD, (a) surfaces
 7 extracted from its adjacent vertebrae, (b) IVD volume created from the two
 8 surfaces, (c) IVD meshes with annulus fibrosus (grey) and nucleus pulposus (blue),
 9 (d) transverse sectional view of the IVD (the boundary between the nucleus
 10 pulposus and annulus fibrosus was marked with blue ink).

11



1
 2 **Figure 3.** (a) Two boundary conditions were simulated for each T12 model: either
 3 pure axial compression was prescribed to the nodes of the superior *PMMA* layer
 4 (*FE-PMMA*) or a 2-stage loading (step 1: 4° forward bending, step 2: axial
 5 compression) was conducted to the nodes of the superior IVD (*FE-IVD*). In both
 6 cases, the bottom nodes of the model were fully constrained. Each T12 model was
 7 discriminated between 4 regions: HR-pQCT based cortical (yellow) and cancellous
 8 bone (blue), annulus fibrosus (grey) and nucleus pulposus (red). (b) Material
 9 heterogeneity of the cancellous bone of a T12 model with bone volume fraction
 10 (BV/TV) and fabric anisotropy.



1

2 **Figure 4.** Linear regressions of the vertebral failure load as a function of the failure
 3 loads predicted by the FE-PMMA (a) and FE-IVD (b) models.

4

5